2014

Experimental Investigation Of An ORC System For A Micro-Solar Power Plant

Rémi Dickes
University of Liège, Belgium, rdickes@ulg.ac.be

Olivier Dumont
University of Liège, Belgium, olivier.dumont@ulg.ac.be

Sébastien Declaye
University of Liège, Belgium, sebastien.declaye@ulg.ac.be

Sylvain Quoilin
University of Liège, Belgium, squoilin@ulg.ac.be

Ian Bell
University of Liège, Belgium, ian.bell@ulg.ac.be

See next page for additional authors

Follow this and additional works at: https://docs.lib.purdue.edu/icec

Authors

Rémi Dickes, Olivier Dumont, Sébastien Declaye, Sylvain Quoilin, Ian Bell, and Vincent Lemort

Experimental investigation of an ORC system for a micro-solar power plant

Rémi DICKES[*], Olivier DUMONT, Sébastien DECLAYE, Sylvain QUOILIN, Ian BELL, Vincent LEMORT

Thermodynamics Laboratory
Aerospace and Mechanical Engineering Department
Faculty of Applied Sciences
University of Liège

* Corresponding Author (rdickes@ulg.ac.be)

ABSTRACT

Because of the depletion of fossil fuels and global warming issues, the world energy sector is undergoing various changes towards increased sustainability. Among the different technologies being developed, solar energy, and more specifically CSP (Concentrated Solar Power) systems are expected to play a key role to supply centralized loads and off-grid areas in the medium-term. Major performance improvements can be achieved by implementing advanced control strategies accounting for the transient and random nature of the solar heat source. In this context, a lab-scale solar power plant has been designed and is under construction for experimental purposes and dynamic analysis. The test rig includes an Organic Rankine Cycle (ORC) unit, a field of parabolic trough collectors and a thermal energy storage system.

This paper presents the results of an experimental campaign conducted on the ORC module alone. This power unit, designed for a 2.8 kW net electrical output, consists of two scroll expanders in series, an air-cooled condenser, a recuperator, a volumetric pump and an oil-heated evaporator. The ORC engine is constructed using standard mass manufactured components from the HVAC industry, this practice reducing considerably the system cost. The overall unit performance and components effectiveness are presented in different operating conditions and relevant empirical correlations are derived to be implemented in a steady state model of the ORC unit.

1. INTRODUCTION

Since the first industrial revolution in the early 19th century, humanity has witnessed an exponential development of societies based on fossil fuels. Consumption of energy resources has led to social benefits as well as tensions on many level: global climate change, exhaustion of oil reserves, destruction of ecosystems and extinction of species are common themes in modern discourse. While ecologically motivated reactions to these tensions began to emerge in the 1960's, by the second decade of the 21th century it has become generally accepted that the development of renewable energy technologies and optimization of energy systems are necessary to ensure a sustainable future for the next generations.

Among the different technologies being developed to this end, Concentrated Solar Power systems is a promising renewable technology. A standard CSP technology uses solar collectors and a tracking system in order to concentrate solar rays during sunshine hours. This concentrated beam is then absorbed and used as the heat source for a thermodynamic cycle. Figure 1 illustrates the working principle of such system using parabolic trough collectors as solar receivers.

The intermittent nature of solar irradiance (day/night, cloudiness) is an inherent drawback of solar technologies which often leads to an imbalance between consumer demand and heat source availability (Manenti and Ravaghi-Ardebili, 2013). However, coupling a cost-effective TES (Thermal Energy Storage) with a CSP system provides the ability to store a certain quantity of energy to be later used during the night or unfavorable meteorological conditions. The whole system is thus more reliable, flexible, effective and can even be an actor in reserve markets (Usaola, 2012).

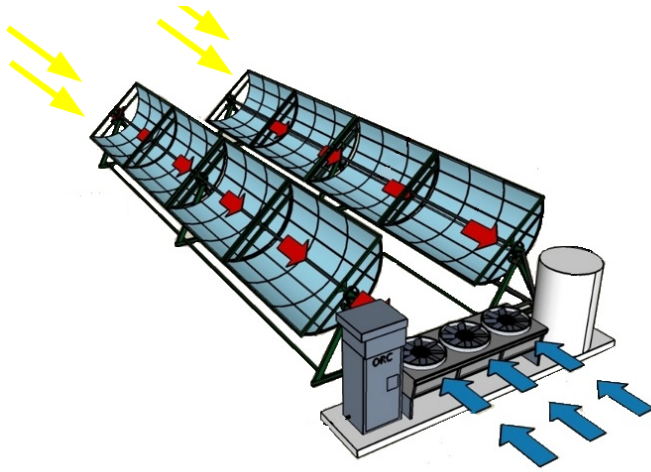In this context,the Thermodynamics Labortory of the University of Liège has worked to design and build a lab-scale

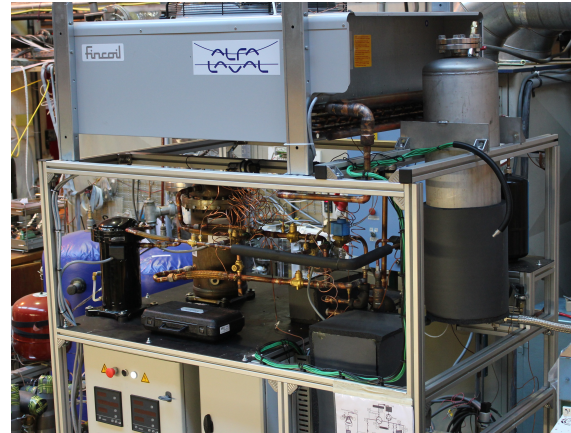**Figure 1: CSP working principle (source: STG International)**

Figure 2: ORC unit test bench

concentrated solar power plant for experimental purposes. The test-rig consists of a 2.8kWe ORC unit (depicted in Figure 2), a pebble-bed heat storage and a field of parabolic trough collectors. This lab-scale system will ultimately be used in control investigation under dynamic and transient operating conditions. In this paper, the ORC unit and its performance are investigated through an experimental campaign.

2. DESCRIPTION OF THE ORC UNIT

In this section, a full description of the ORC engine and its architecture is provided. After a brief reminder of the thermodynamic cycle principle, components constituting the engine and the data acquisition system are described. The ORC engine is constructed using standard mass manufactured components from the HVAC industry, this practice reducing considerably the system cost.

2.1 The Organic Rankine Cycle
In comparison with photovoltaics which directly convert solar energy to electricity, concentrated solar power plants use sunlight as a heat source to supply a power generating thermodynamic system (generally a *Rankine* cycle). This Rankine cycle aims to convert heat into mechanical work by means of a working fluid that undergoes a closed-loop process illustrated in Figure 3. First, the working fluid at a saturated liquid state is pressurized by a pump and then vaporized to a superheated state in an evaporator. The superheated vapor is next expanded through an expansion device which is connected to a generator producing the electricity. The residual energy of the working fluid at the expander outlet is transferred through a recuperator in order to preheat the liquid fluid between the pump and the evaporator. Finally, the working fluid is cooled down thanks to a condenser and heat is released to the environment.

Although water is the most commonly used working fluid in a Rankine cycle, organic fluids are more suitable in low grade heat applications because of their interesting thermo-physical properties at low temperature (Quoilin, 2011). In such case, the thermodynamic cycle is known as an Organic Rankine Cycle or *ORC*. For this application, HFC-245fa (pentafluoropropane) has been chosen as working fluid for the organic Rankine cycle and the nominal operating conditions of the ORC unit are summarized in Table 1. The whole design process of this test bench, including the cycle architecture definition and the components/fluid selection is described by Georges et al. (2013).

2.2 Pumps
Among the different types of volumetric pumps, both a gear pump (model: Viking SG-80550-M0V)) and a multi-diaphragm pump (model: Hydra-Cell G-13) are tested to pressurize the working fluid in the ORC. In order to control the working fluid mass flow rate, a variable frequency drive is used to regulate the pump shaft speed. The pumps per-

Table 1: ORC nominal operating conditions

ORC nominal operating conditions		
Working fluid	HFC-245fa	
Heat transfer fluid	Thermal oil	
Refrigerant mass flow rate	0.105	$kg.s^{-1}$
Evaporating temperature	140	°C
Evaporating pressure	28	bar
Evaporator thermal power	24	kW
Condensing temperature	35	°C
Condensing pressure	2.1	bar
Condenser thermal power	20.5	kW
Recuperator themal power	3.5	kW
Pump consumption	0.3	kW
Net power output	2.8	kW
Cycle efficiency	11	%

formance is evaluated through their isentropic and volumetric efficiencies, respectively defined in Eqs. 1 and 2,

$$\eta_{is,pp} = \frac{\dot{m}(h_{ex,is,pp} - h_{su,pp})}{\dot{W}_{pp,elec}} \tag{1}$$

$$\eta_{vol,pp} = \frac{\dot{V}_{meas,pp}}{\dot{V}_{th,pp}} \tag{2}$$

where $\dot{V}$ is the volumetric refrigerant flow rate, $\dot{W}_{pp,elec}$ is the electrical power consumption of the pump and $\dot{m}$ is the refrigerant mass flow rate.

2.3 Expanders

The expansion process is performed by two positive displacement expanders. The scroll technology is chosen because of its low cost, reliability, robustness, good efficiency and mechanical simplicity, which makes it well suited for an ORC application (Dickes, 2013). However, a major drawback of scroll machines is their relatively small intrinsic volume ratio ($r_{v,in}$ ~ 2.5) in comparison to the ORC operating conditions ($r_{v,ORC}$ ~ 15). This limits the ORC operating range of application, or generates under-expansion losses, both cases resulting in a drop of the power plant efficiency. To overcome this problem, two scroll expanders in series are used to achieve an expansion ratio closer to the ORC nominal working conditions (Georges et al., 2013). To this end, two scroll compressors from Copeland, respectively a *ZR34K3E-ZD* and a *ZR144KCE-TFD* for the high pressure and low pressure expansions, have been modified to run in reverse as expanders. The two scroll expanders are directly connected to the grid, their shaft speed remains therefore constant (3000 rpm). The expander performance is evaluated through its isentropic efficiency $\eta_{is,exp}$ and its filling factor *FF* (Zanelli and Favrat, 1994) given in Eqs. 3 and 4.

$$\eta_{is,exp} = \frac{\dot{W}_{exp,elec}}{\dot{m}(h_{su,exp} - h_{ex,is,exp})} \tag{3}$$

$$FF = \frac{\dot{V}_{meas,exp}}{\dot{V}_{th,exp}} \tag{4}$$

2.4 Condenser

The system is designed assuming that there is not water available for cooling purpose on site. Therefore, an air-cooled fin coil condenser *SOLAR Junior 121* from Alfa Laval has been selected to cool down the working fluid and to release heat to the environment. Cooling capacity is regulated through the fan speed which is controlled thanks to a VFD (Variable Frequency Drive).
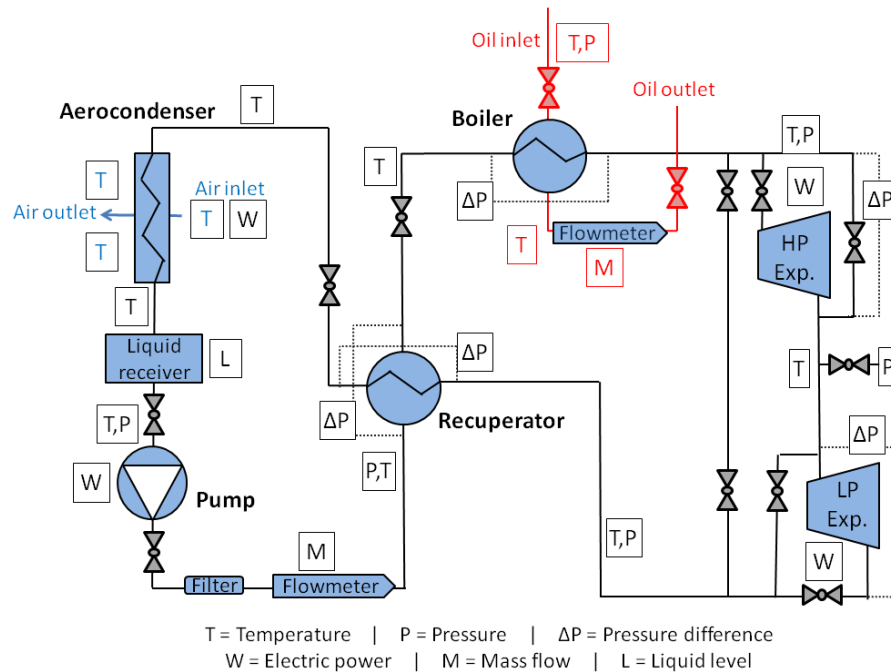
T = Temperature | P = Pressure | ΔP = Pressure difference
W = Electric power | M = Mass flow | L = Liquid level

Figure 3: ORC cycle and sensors location

2.5 Evaporator and recuperator

The evaporator consists of a single brazed plate heat exchanger used to preheat, vaporize and superheat the working fluid. It is fed with thermal oil coming from an electric boiler replacing the solar loop during this experimental campaign. The model selected for this application is the *CB76-100E* plate heat exchanger developed by Alfa Laval. Furthermore, a smaller model of brazed plate heat exchanger, i.e. the *CB30-40H-F* from Alfa Laval, is selected for the recuperator.

2.6 Measurements setup and acquisition system

The operating diagram of the test rig with the different measurement sensors is given in Figure 3. Temperatures are measured by T-type thermocouples and the pressures are measured with gage, absolute and differential pressure sensors. A Coriolis flow meter is used to evaluate the refrigerant flow rate in the ORC and the electrical power consumption/generation of the different components is measured by four wattmeters. The measurement acquisition is performed by a CompactRIO (National Instrument, model: cRIO-9022) interacting with a LabView interface which displays the real-time performance. This LabView interface also permits the operator to control remotely the test bench. Data collected after the experimental run (T, P, mass flow, etc.) are post-processed in a steady-state model developed in EES to derive the ORC performance ($\dot{Q}_{ev}$, $\eta_{is,pp}$, FF_{exp}, etc.) .

Table 2 summarizes the different components and measurement sensors constituting the ORC test rig.

3. EXPERIMENTAL CAMPAIGN

More than 110 steady-state performance points are measured by varying the operating conditions, i.e. the evaporating and condensing pressures, the refrigerant and oil mass flow rates, the heat source temperature and the condenser fan and pump shaft speed. Table3 provides the maximum and minimum values of these operating parameters achieved during the experimental campaign. These data are used to characterize the cycle and its components effectiveness. The results will be used to calibrate a steady-state model of the ORC in order to extrapolate its performance through a wide operating range. The following section presents main results derived from this experimental campaign.

Table 2: Components and sensors summary

Sensor type	Brand	Model
Absolute pressure sensor	Keller	PA-21y
Gauge pressure sensor	Keller	PAA-21y
Differential pressure sensor	Sistans	P, DS III
Coriolis flow meter	Krohne	Optimass 7000
Wattmeter	GMC	A2000
Component	**Brand**	**Model**
Expander HP	Copeland	ZR34K3E-ZD
Expander LP	Copeland	ZR144KCE-TFD
Gear pump	Viking	SG-80550-M0V
Diaphragm pump	Hydra-cell	G-13
Condenser	Alfa Laval	SOLAR Junior 121
Evaporator	Alfa Laval	CB76-100E
Recuperator	Alfa Laval	CB30-40H-F

Table 3: Maximum and minimum values for the main operating parameters

Parameter	min	max	
P_{ev}	14.5	22.6	bar
P_{cd}	2.1	7.9	bar
$T_{ev,ex}$	111	135	°C
$T_{cd,ex}$	25.8	61.8	°C
$\dot{m}_{R245fa}$	76.2	149	g/s
$\dot{Q}_{ev,th}$	14.6	29.5	kW
$\dot{Q}_{cd,th}$	14.6	29.5	kW
$\dot{W}_{exp,elec}$	0.57	1.78	kW
$\dot{W}_{pp,elec}$	0.28	0.7	kW

3.1 Pump performance

The two pumps efficiencies are evaluated for different mass flow rates and different pressure ratios, as illustrated in Figure 4 for the gear pump. The higher the pressure ratio, the greater the internal leakages, which results in a lower pump volumetric effectiveness. The isentropic efficiency, on the other hand, increases with the pressure ratio. Finally, as it can be seen, better results are achieved with a higher pump shaft speed.

From these experimental data, third order polynomial correlations characterizing the pump efficiencies (in function of the pressure ratio, the pump shaft speed and its NPSH) are defined. These equations will be integrated in the ORC model to extrapolate the pump performance in any other operating conditions.

3.2 HP expander performance

The expander's performance is also investigated experimentally for different operating conditions. In this manuscript, only results related to the high pressure (HP) expander (i.e. a Copeland ZR34K3E-ZD modified to run in reverse) are provided, experiments on the low pressure (LP) expander are still ongoing on the test rig.

The HP expander isentropic efficiency and filling factor are evaluated as a function of the pressure ratio for different mass flow rates and supply pressures. An example of performance is depicted in Figure 5 illustrating the aforementioned efficiencies with a refrigerant mass flow rate of 110 *g/s* and supply pressure of 18.6 *bar*. For the first 45 data points, experimental data regarding the expander exhaust pressure was lacking. This pressure has been recalculated by properly identifying the pressure drop between this point and the pressure sensor downstream for the data points where data is available. Only results derived by correct measurements are presented in this manuscript.

3.3 Air-cooled condenser performance

Two important properties characterizing the condenser, i.e. its electrical consumption and its volumetric air flow rate, are evaluated for different fan speed. The air flow rate is measured at the condenser outlet with an anemometer. From these measurements, two polynomial interpolations illustrated in Figure 6 are derived i.e.

$$\dot{W}_{cd,elec} = 0,1059 \cdot f_{cd}^2 - 0,0647 \cdot f_{cd} + 16,504 \tag{5}$$

$$\dot{V}_{cd,air} = -2 \cdot 10^{-6} \cdot f_{cd}^3 - 0,0003 \cdot f_{cd}^2 + 0,0471 \cdot f_{cd} - 0,0977 \tag{6}$$

where f_{cd} is the condenser frequency. These equations will be included to the ORC model in order to simulate the air-cooled condenser performance in any other operating conditions.

3.4 Pressure drops

Pressure drops in the heat exchangers and relevant piping sections are measured for different refrigerant volumetric flow rates. From these experimental results, a linear correlation is defined for each pressure drop i.e.

$$\Delta P_{drop} = K \cdot \varphi + B \tag{7}$$

$$\varphi = \frac{\dot{m}^2}{\rho} \tag{8}$$

where ρ is the mean refrigerant density and φ is the refrigerant kinetic energy. In the case of multi-phase components (i.e. the condenser or the evaporator), the refrigerant density is evaluated in the vapor zone because the liquid influence is negligible. Pressure drops and their respective linear correlations are illustrated in Figure 7. As for the other aforementioned experimental results, these empirical correlations will be also integrated in the ORC model.

3.5 T-s diagram and best performance

In order to compare the nominal working conditions of the ORC with actual experimental performance, T-s diagrams of both cases are illustrated in Figure 8. The green dotted line is the ideal working conditions derived from design expectations whereas the red solid line represents actual experimental data of a steady state point. Although the comparison is truncated because only a single expander is used experimentally, interesting observations can be made.

Among them, it can be seen that the highest expander isentropic efficiency is lower than the design nominal expectations (70% vs 68%). Indeed, one can observe that expansion slope on the T-s digram is less steep than it should be in theory (5 → 6). Furthermore, a significant pressure drop occurs in the low pressure line connecting the expander exhaust to the recuperator (6 → 7). This pressure loss is due to piping elbows and excessive throttling losses. Thermal losses
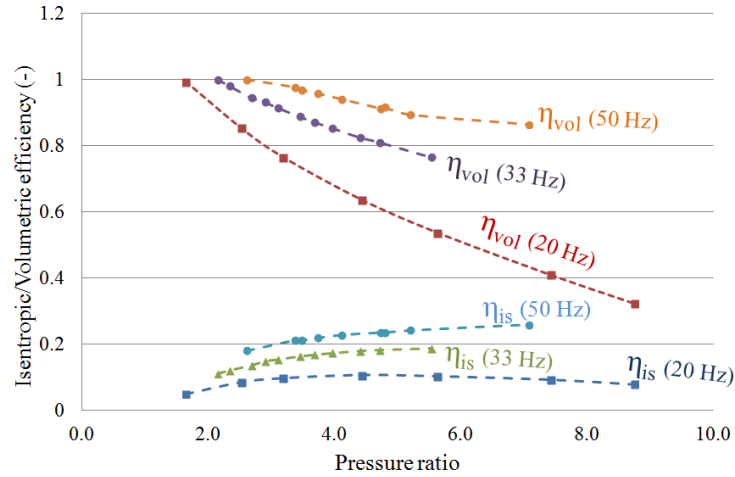
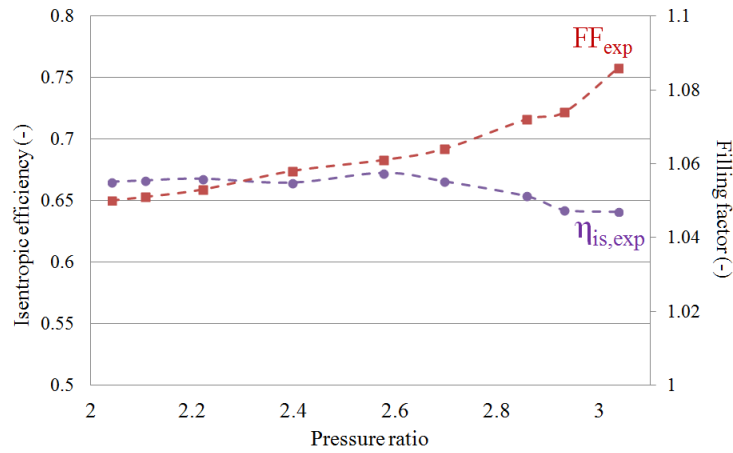**Figure 4: Gear pump efficiencies in function of the pressure ratio (at 20, 33 and 50 Hz)**

Figure 5: Filling factor and isentropic efficiency of the HP expander in function of the pressure ratio ($\dot{m}$ = 110 g/s and $P_{exp,su}$ = 18.6 bar)
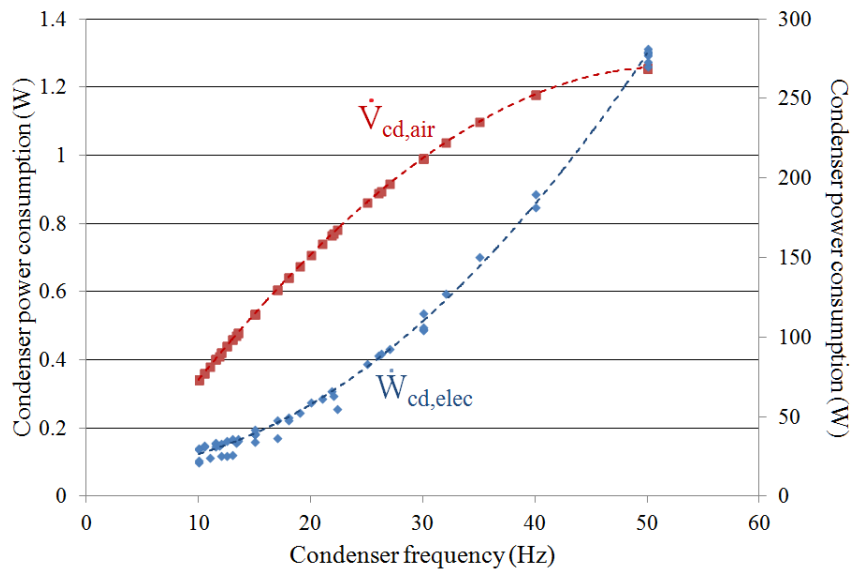

Figure 6: SOLAR Junior air cooled condenser performance in function of the fan frequency
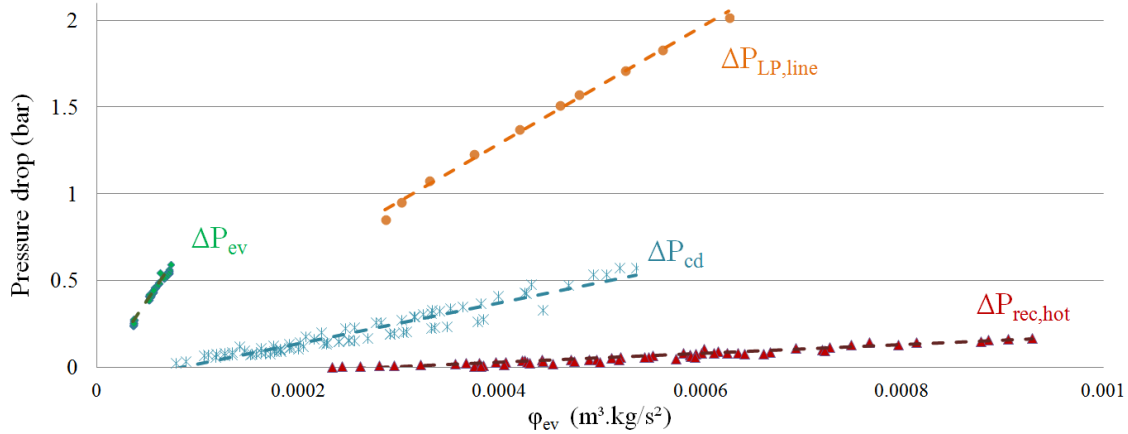
Figure 7: Pressure drops in function of the refrigerant kinetic energy - in the evaporator (green), the low pressure line (orange), the condenser (blue) and in the hot-side of the recuperator (red)
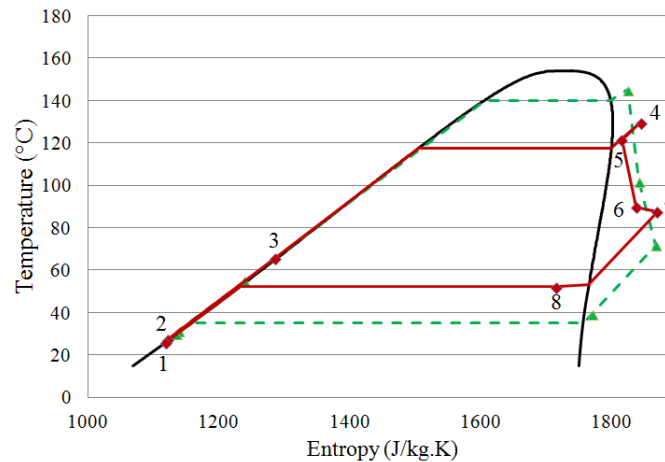

Figure 8: Comparison between design nominal working conditions (green doted line) and experimental performance (red plain line)

also occur between the evaporator and the expander (4 → 5) due to the absence of insulation on the pipes. Finally, it can be seen that the refrigerant partly condenses in the recuperator (7 → 8) instead of the condenser. This results in a higher condensing pressure and an excessive subcooling at the condenser outlet. These phenomena can be explained by an excessive quantity of refrigerant in the cycle, this hypothesis being confirmed by the fact that the liquid receiver remains filled by liquid during the whole experimental campaign.

Highest-performance points are given in Table 4. A maximum expander power generation of 1780 W is achieved and the maximum cycle net power output is 915 W. Satisfactory performance of the expander is observed with a best isentropic efficiency of 68% and a filling factor equal to 105%. In addition to these results, Figure 9 depicts the *thermally normalized electrical power* for each component, as defined in Eq. 9, for 46 different operating conditions.

$$\dot\omega_{pp} = \frac{\dot W_{pp,elec}}{\dot Q_{ev}} \qquad \dot\omega_{exp} = \frac{\dot W_{exp,elec}}{\dot Q_{ev}} \qquad \dot\omega_{cd} = \frac{\dot W_{cd,elec}}{\dot Q_{ev}} \qquad \dot\omega_{net} = \frac{\dot W_{net,elec}}{\dot Q_{ev}} = \eta_{cycle} \qquad (9)$$

On this diagram, each column corresponds to a steady state operating point and illustrates the relative importance of electrical consumption of the pump and the condenser fan over the expander power generation. It can be seen that

Table 4: Highest-performance points

Highest expander isentropic efficiency	68	%
Highest expander filling factor	105	%
Highest cycle efficiency	4.5	%
Highest expander power generation	1780	W
Highest ORC net power generation	915	W
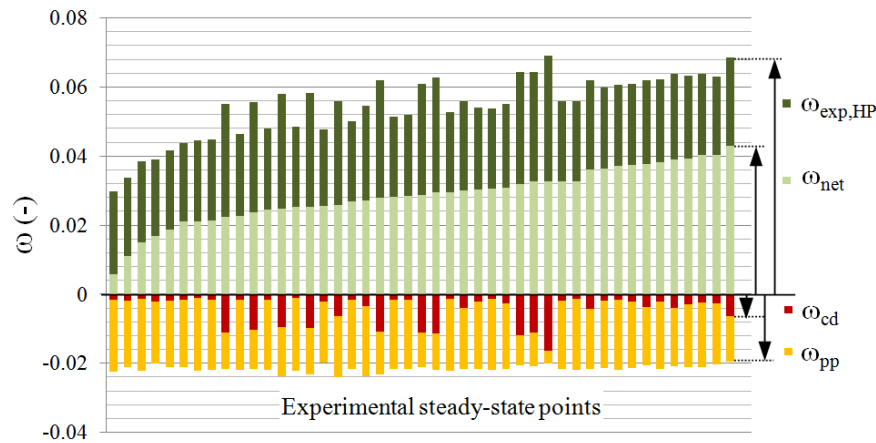
Figure 9: Thermally normalized electrical powers for 46 different operating conditions (sorted by increasing cycle efficiency)

the major internal power consumption is due to the pump whereas the condenser fan fraction remains marginal in most of the cases. Moreover, the pump consumption is proportional to the evaporator thermal power in any case. The fan power is independent of this parameter and influences mainly the expander power generation. Indeed, the higher the fan consumption, the higher the cooling capacity, the condensing pressure is thus decreased resulting in a higher expander power output. However, the fan consumption does not influence significantly the net power generation of the ORC unit since the additional power generated by the expander is consumed by the air-cooled condenser. Therefore, the optimal cooling capacity is defined from a trade-off between the additional power generated by the expander and the extra electrical consumption of the condenser fan.

4. CONCLUSION

This manuscript presents a 2.8 kWe ORC engine developed at the University of Liège to be integrated in a micro-solar power plant. First, the components and the measurement system constituting the ORC are described and performance indexes are defined. Then, from data derived experimentally, relevant properties characterizing the main components are presented. Experimental correlations are defined to simulate the components performance in function of the operating conditions in order to be integrated in a steady state model of the ORC unit.

Prospective works include to finish the experimental characterization of the low pressure expander. The next step will be to run the two expanders in series in order to meet the design expectations of the test rig. Technical improvements on the test bench have also to be done, such as to insulate thermally all the pipes and to reshape the low pressure line in order to decrease the pressure drop occurring in this section. Afterward, the ORC engine will be coupled with the solar loop of the micro-CSP plant and dynamic control strategies will be investigated to optimize the power generation under transient operating conditions. In order to define the optimal operating conditions of the ORC in any situation (pump shaft speed, cooling capacity, one or two expanders connected, etc.), a calibrated empirical model of the test rig will be used to investigate its performance over a wide range of operating conditions.

5. ACKNOWLEDGMENT

NOMENCLATURE

Acronyms		Symbols		Subscripts	
CSP	Concentrated Solar Power	h	enthalpy	cd	condenser
FF	Filling Factor	f	frequency	elec	electric
HP	High Pressure	$\dot{m}$	mass flow	ev	evaporator
LP	Low Pressure	P	pressure	ex	exhaust
ORC	Organic Rankine Cycle	r_v	volumetric ratio	exp	expander
PTC	Parabolic Through Collector	s	entropy	is	isentropic
TES	Thermal Energy Storage	T	temperature	in	internal
VFD	Variable Frequency Drive	$\dot{V}$	volumetric flow	meas	measured
		Δ	difference	pp	pump
		φ	kinetic energy	su	supply
		ρ	density	th	theoretical
				vol	volumetric

REFERENCES

Dickes, R. (2013). Design and fabrication of a variable wall thickness two-stage scroll expander to be integrated in a micro-solar power plant. Master's thesis, University of Liège.

Georges, E., Declaye, S., Dumont, O., Quoilin, S., and Lemort, V. (2013). Design of a small-scale orc engine used in a solar power plant. *Internation Journal of Low-Carbon Technologies*.

Manenti, F. and Ravaghi-Ardebili, Z. (2013). Dynamic simulation of concentrating solar power plant and two-thanks direct thermal energy storage. *Energy*.

Quoilin, S. (2011). *Sustainable energy conversion through the use of organic Rankine cycles for waste Heaht recovery and solar applications*. PhD thesis, University of Liège.

Usaola, J. (2012). Participation of csp plants in the reserve markets: A new challenge for regulators. *Energy policy*.

Zanelli, R. and Favrat, D. (1994). Experimental investigation of a hermetic scroll expander-generator. *International compressor engineering conference*.